Chemistry–A European Journal
Research Article
doi.org/10.1002/chem.202203980
Chemistry Europe
European Chemical Societies Publishing
www.chemeurj.org

An Air- and Moisture-stable Zinc(II) Carbene Dithiolate Dimer Showing Fast Thermally Activated Delayed Fluorescence and Dexter Energy Transfer Catalysis**

Ondřej Mrózek,[a] Mousree Mitra,[a] Bejamin Hupp,[a] Andrey Belyaev,[a] Nora Lüdtke,[b] Dorothee Wagner,[c] Cui Wang,[c] Oliver S. Wenger,[c] Christel M. Marian,*[b] and Andreas Steffen*[a]

Abstract: A dimeric Zn^{II} carbene complex featuring bridging and chelating benzene-1,2-dithiolate ligands is highly stable towards air and water. The donor-Zn-acceptor structure leads to visible light emission in the solid state, solution and polymer matrices with λ_{max} between 577–657 nm and, for zinc(II) complexes, unusually high radiative rate constants for triplet exciton decay of up to $k_r = 1.5 \times 10^5\ s^{-1}$ at room temperature. Variable temperature and DFT/MRCI studies show that a small energy gap between the $^{1/3}$LL/LMCT states of only 79 meV is responsible for efficient thermally activated delayed fluorescence (TADF). Time-resolved luminescence and transient absorption studies confirm the occurrence of long-lived, dominantly ligand-to-ligand charge transfer excited states in solution, allowing for application in Dexter energy transfer photocatalysis.

Introduction

Photoactive complexes of the 3d elements are currently being intensively investigated[1–6] with regard to their potential to either substitute or complement more precious 4d/5d transition metal complexes in photonic applications, where triplet excitons need to be harvested. The exploitation scenarios include, for example, sensors,[7] imaging,[8] organic light emitting devices (OLEDs),[9,10] stimuli-responsive materials,[11] as well as photocatalysis[5,12–14] for high-value products. Besides the argument of relative costs of the metals, one of the major driving forces for this development is certainly also the desire to understand the spin dynamics and various luminescence phenomena, and to discover new photoreactions. Ultimately, the breadth of findings will lead to the formulation of structure-property relationships, allowing for control of the photophysical and -chemical properties for a given application scenario. For many of the first-row transition metal complexes in their d^1 to d^9 electron configuration, an important intellectual challenge to realize room-temperature luminescence is the occurrence of metal-centred (MC) d–d* states,[15] which can be populated thermally from the initial excited states of charge transfer (CT) character and often lead to undesired non-radiative decay. Strategies to overcome this problem are to increase the ligand field splitting[16,17] or manipulate the energy of CT states[18] by judicious choice of the ligand sphere.

An alternative is to employ metal centres in their d^0 or d^{10} electron configuration.[10,18–23] This approach provides the additional advantage of various coordination spheres of the same metal centre being accessible, which greatly influences the nature, energy and reactivity of the excited states. Extensive work on trigonally and linearly coordinated Cu^I compounds, in particular, has shown that very efficient triplet state decay can be obtained either by phosphorescence,[20,24–26] or thermally activated delayed fluorescence (TADF).[10,21,27–29] For this, the ideal molecular structure should allow for the formation of low-energy ligand-to-ligand charge transfer (LLCT) states with some metal-to-ligand (ML)CT admixture to mediate spin-orbit coupling (SOC). While Cu^I is beneficially redox-active, the high oxidation potential of Zn^{II} forbids the formation of MLCT states. In addition, the majority of photoactive zinc(II) complexes is homoleptically coordinated, and thus fluorescent from ligand-centred (^{1}LC) states.[30–32]

[a] Dr. O. Mrózek, M. Mitra, Dr. B. Hupp, Dr. A. Belyaev, Prof. Dr. A. Steffen
Department of Chemistry and Chemical Biology
TU Dortmund University
Otto-Hahn-Str. 6
44227 Dortmund (Germany)
E-mail: andreas.steffen@tu-dortmund.de

[b] N. Lüdtke, Prof. Dr. C. M. Marian
Institute of Theoretical and Computational Chemistry
Heinrich Heine University Düsseldorf
40225 Düsseldorf (Germany)
E-mail: Christel.Marian@hhu.de

[c] D. Wagner, Dr. C. Wang, Prof. Dr. O. S. Wenger
Department of Chemistry
University of Basel
4056 Basel (Switzerland)

[**] A previous version of this manuscript has been deposited on a preprint server (https://doi.org/10.26434/chemrxiv-2022-j0rbs)

Supporting information for this article is available on the WWW under https://doi.org/10.1002/chem.202203980

However, a class of heteroleptically coordinated [ZnX_2(phen)] (phen = 1,10-phenanthroline; X = halides, thiolates) has been reported to exhibit rare, but very weak phosphorescence at room temperature from ^{3}LLCT/^{3}LC(phen) states.[33] We recently refined this analysis by extensive theoretical and experimental studies, showing that, in fact, TADF occurs from $^{1/3}$LLCT states with a very small energy gap $\Delta E(S_1\text{-}T_1)$, although non-radiative deactivation is dominant.[34] A similar behaviour was described for a zinc(II) iminophosphonamide complex by Roesky et al.[35] Adachi and co-workers reported TADF from a homoleptically coordinated Zn^{II} compound, albeit low radiative rate constants of only $k_r = 2.6\times10^4\ s^{-1}$ from intra-ligand $^{1/3}$(IL)CT states were found.[36]

These rare examples show that there is indeed potential to exploit zinc(II) complexes for triplet exciton harvesting via TADF, and we thus followed the strategy of preparing donor-M-acceptor structures to enter $^{1/3}$LLCT states to ensure high k_r. As a first foray into this field, we recently employed an electrophilic cyclic alkyl(amino)carbene (cAAC) as acceptor site for Zn^{II} halides, with the latter acting as donors. The obtained dimers [$Zn_2Cl_2(\mu\text{-}Cl)_2(^{Me}cAAC)_2$] feature triplet ^{3}XCT/LE excited states with ultra-long lifetimes up to several milliseconds, but undesired photo-induced conformational transformation as well as further decomposition processes at room temperature involving the Zn–X bonds was observed.[37] In order to enhance the stability and foster the formation of low-energy LLCT excited states, we now focused on chelating benzene-1,2-dithiolate (bdt) as a redox-active donor for the {Zn(^{Me}cAAC)} acceptor motif.

Results and Discussion

The reaction of two equivalents disodium benzene-1,2-dithiolate (Na_2bdt) with [$Zn_2Cl_2(\mu\text{-}Cl)_2(^{Me}cAAC)_2$][37] in THF solution occurs with a fast color change from colorless to yellow and simultaneous precipitation of NaCl (Figure 1). After work-up, crystallization using a CH_2Cl_2/*n*-pentane mixture afforded yellow single crystals of **Zn1** in 74% isolated yield. X-ray diffraction analysis revealed a centrosymmetric, dimeric arrangement, in which the bdt units each bind with one sulfur solely to one zinc(II) ion and bridge the two {Zn(^{Me}cAAC)} fragments with the other (Figure 1).

Although a similar coordination mode of bdt was reported for electron-deficient Zn^{II} complexes bearing *N*,*N*-chelating ligands,[38,39] it is unprecedented in the context of carbene compounds, and we find that the Zn-$S^{bridging}$ distances are slightly shorter by ~0.07 Å for **Zn1**. The Zn–$C^{carbene}$ bond length of 2.0575(13) Å is very similar to the value found for [$Zn_2Cl_2(\mu\text{-}Cl)_2(^{Me}cAAC)_2$] of 2.0547(17) Å. We note that the dimeric structure of **Zn1** is maintained in solution as the ^{1}H and $^{13}C\{^1H\}$ NMR spectra show only one set of sharp signals.

The μ_2,k^2-bonding mode of the bdt ligands is a key feature of the molecular structure and provides enhanced steric protection of the Zn–C(carbene) bond of **Zn1** in comparison to the chloride bridged congener[37], which is highly photolabile at room temperature even in the solid state, and highly sensitive towards oxygen and moisture. In contrast, **Zn1** is remarkably photostable not only in the solid state, but more importantly also in dry and de-oxygenated, or aerated and wet CD_2Cl_2 solution (Figure S6 in Supporting Information). Notably, no protonation of ^{Me}cAAC or bdt ligands was observed in the presence of water, which is surprising as carbene complexes are typically prone to hydrolysis even in the presence of traces of moisture in organic solvents. TGA/DSC measurements indicate good thermal stability as single-crystalline **Zn1** decomposes only above 210 °C by dissociation of one ^{Me}cAAC ligand after first liberating 2 equivalents of co-crystallized solvent (Figure S5).

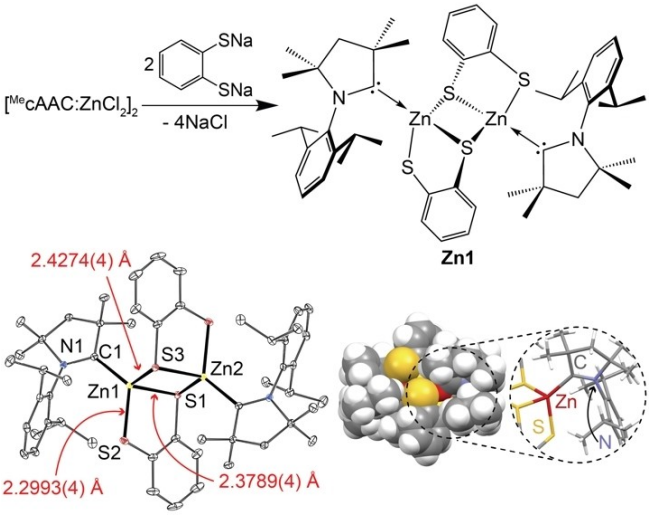

Figure 1. Synthesis and crystal structure of **Zn1**. Thermal ellipsoids are drawn at the 30% probability level and hydrogens are omitted for clarity. Selected bond lengths (Å) and angles (°): Zn1-C1 2.0575(13); Zn1-S1 2.3789(4); Zn1-S2 2.2993(4); Zn1-S3 2.4274(4); C1-Zn1-S1 115.47(4); C1-Zn1-S2 125.36(4); C1-Zn1-S3 119.58(4); Zn1-S1-Zn2 80.83(1); S1-Zn1-S3 99.17(1).

Cyclic voltammetry (CV) on **Zn1** performed in acetonitrile using the ferrocene/ferrocenium couple as a reference revealed a series of irreversible oxidation events within the potential range of 0.2–1.5 V (Figure S7) that we assign to consecutive oxidations of the thiolate moieties. As a consequence, thiyl radicals can be formed that have a strong tendency to dimerize to give disulfide species,[40] which can easily dissociate from the zinc(II) centers and thus explain the irreversible character of the oxidative events. In addition, we observed a fully reversible reduction wave at −2.35 V associated with the reduction of the ^{Me}cAAC ligand as shown by DFT calculations (Figure 2).

The UV/vis absorption spectra of **Zn1** in CH_2Cl_2 solution display a broad low-energy band with $\lambda_{max} = 374$ nm (ε = 3,600 $M^{-1}cm^{-1}$), which stems from bdt(π)→^{Me}cAAC(π^*_{CN}) LLCT excitations with LMCT admixture according to our DFT/MRCI calculations (Figures 2 and 3). In the inversion-symmetric minimum nuclear arrangement of the electronic ground state, only the $S_0\rightarrow S_2$ and $S_0\rightarrow S_3$ transitions, both of $^1A_g\rightarrow{}^1A_u$ type, carry nonvanishing but small electric dipole oscillator strengths of 0.02 and 0.05, respectively, which are in line with the observed weak absorption. Vibronic interactions, which lift the

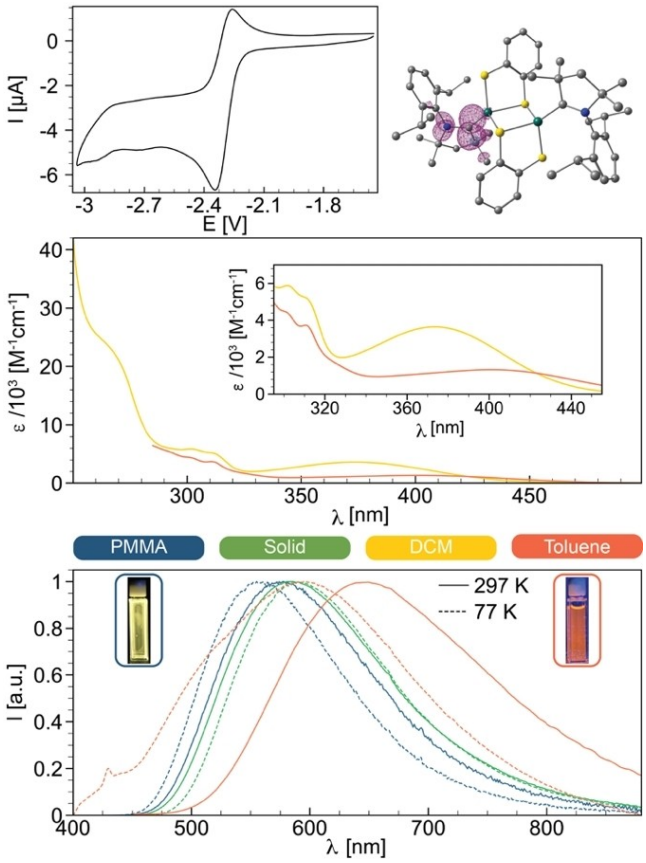

Figure 2. Top: CV vs. Fc/Fc^+ in CH_3CN using an Ag reference electrode (left) and calculated spin density (right) of the radical anion **Zn1**$^-$. Middle: absorption spectra of **Zn1** in CH_2Cl_2 (yellow) and toluene (orange). Bottom: emission spectra of **Zn1** in PMMA, solid state, CH_2Cl_2 and toluene at 297 (solid lines) and 77 K (dashed lines).

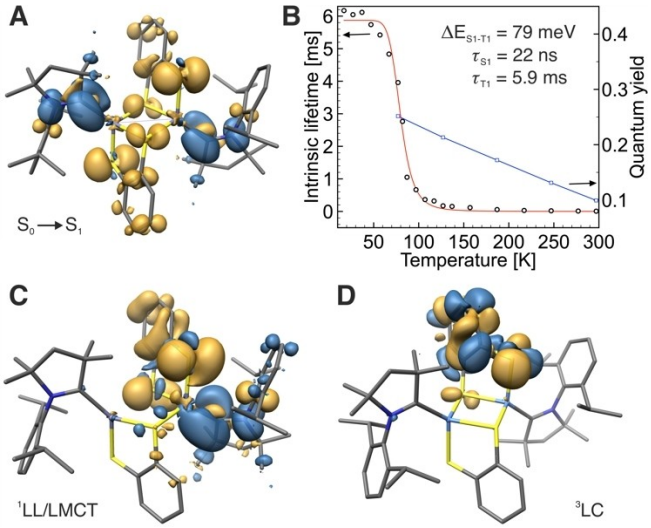

Figure 3. DFT/MRCI difference densities (isovalue ±0.0015) of the $S_0 \rightarrow S_1$ absorption (A), and of the optimized ^{1}LL/LMCT (C) and ^{3}LC (D) states of **Zn1** in THF. Areas losing electron density upon electronic excitation from the ground state are shown in gold, areas gaining electron density in blue. Experimental TADF fit of **Zn1** in PMMA (B).

symmetry selection rules, are expected to lend intensity to the $S_0 \rightarrow S_1$ and $S_0 \rightarrow S_4$ transitions as well, thus broadening the band in the low-energy regime. The high-energy region of the spectrum shows a series of additional absorptions including rather broad bands centred at 306 (structured, $\varepsilon \sim$ 5,500 $M^{-1}cm^{-1}$), 267 ($\varepsilon =$ 23,000 $M^{-1}cm^{-1}$) and 243 nm ($\varepsilon =$ 37,600 $M^{-1}cm^{-1}$), respectively. The first transition, calculated at 301 nm in THF, originates from an intra-ligand (IL)CT on bdt involving sulfur lone-pair orbitals as donors and the benzene π system as acceptor (Figure S25). The band with $\lambda_{max} = 267$ nm consists of several strong transitions with varying LLCT and ILCT contributions. Here, charge is transferred from sulfur lone pairs to π* orbitals of the ^{Me}cAAC ligand or of the benzene unit of btd. At the blue edge of this band, the first bdt→Rydberg transition, involving 3d shells of the sulfur atoms, is encountered in the DFT/MRCI spectrum. Complex **Zn1** further features additional strong and high-energy absorptions shown as two narrow bands at 248 and 236 nm ($\varepsilon \sim$ 53,000 $M^{-1}cm^{-1}$) that can be assigned to LC transitions of π→π* character localized at the bdt unit (Figure S26). The absorption features in toluene solution are very similar, but λ_{max} of the lowest energy band shifts bathochromically by 27 nm (1,800 cm^{-1}) due to the lower solvent polarity in comparison to CH_2Cl_2 (see below), which is beneficial for utilization of **Zn1** in photocatalysis.

Upon photoexcitation ($\lambda_{ex} =$ 360–480 nm), broad luminescence with $\lambda_{max} = 648$ nm is observed in de-aerated CH_2Cl_2 at room temperature, albeit with low quantum yield $\phi_{PL} = 0.02$ (Figure 2 and Table 1). The observed emission lifetime of 135 ns gives rise to $k_r = 1.5 \times 10^5$ s^{-1}, indicative of triplet states being involved.[6,20–26] However, k_r is too fast for phosphorescence as SOC mediated by the zinc and sulfur atoms would be too small, and thus we assign the emission to TADF. We note a minor negative solvatochromic shift in toluene by 164 cm^{-1}, that might be related to the centrosymmetric nature of **Zn1** in its ground state. In both solvents, large Stokes shifts of 9,700–11,300 cm^{-1} are caused by unhindered geometry relaxation in the S_1 and T_1 state accompanied by substantial nuclear displacements and localization of the CT excitation on one side of the complex according to our calculations (Figure 3C). Consequently, facile vibrational relaxation S_1/T_1S_0 is possible, explaining the low ϕ_{PL} and short τ. This structural distortion is

Table 1. Photophysical data for **Zn1** in solid state, solutions, and polymeric matrices.

Medium	T [K]	λ_{max} [nm]	τ [ns][a]	Φ_{PL}	k_r [s^{-1}][b]	k_{nr} [s^{-1}][c]
solid	297	585	472	0.02	4.2×10^4	2.1×10^6
	77	587	170×10^3	0.06	35.2	552
crystals	297	644	97	> 0.01	–	–
	77	639	260×10^3	0.01	38.5	3810
DCM	297	650	135	0.02	1.5×10^5	7.3×10^6
	77	551	316×10^3	–	–	–
Toluene	297	657	194	0.02	1.0×10^5	5.1×10^6
	77	596	641×10^3	–	–	–
PS	297	585	444	0.02	4.5×10^4	2.2×10^6
	77	580	927×10^3	0.08	86.3	993
PMMA	297	577	741	0.10	1.4×10^5	1.2×10^6
	77	558	987×10^3	0.25	253.0	760

[a] amplitude average lifetime, [b] $k_r = \phi_{PL}/\tau$, [c] $k_{nr} = (1-\phi_{PL})/\tau$.

hindered in the solid state or in polystyrene (PS) matrix, and thus the emission shifts hypsochromically to $\lambda_{max}=585$ nm (Table 1). Interestingly, **Zn1** in PMMA matrix (10 wt-%) shows an even larger hypsochromic shift of 1,946 cm^{-1} compared to CH_2Cl_2 solution to $\lambda_{max}=577$ nm. In addition to the enhanced rigidity (see above), the polar environment stabilizes the polar ground state of **Zn1** with negatively charged bdt ligands and positively charged Zn^{II}/^{Me}cAAC, further increasing the energy gap $\Delta E(S_1\text{-}S_0)$. These effects lead to greatly enhanced $\phi_{PL}=0.10$ while maintaining the high k_r. In order to shed light on the assumed TADF mechanism, we performed detailed variable-temperature (VT) measurements in PMMA, in which **Zn1** exhibits the most efficient luminescence (Figures 2 and 3). Upon lowering the temperature to 77 K, the yellow emission shifts hypsochromically by ca. 20 nm due to further rigidification, with a concomitant increase of τ to 987 µs. The intrinsic radiative lifetimes $\tau_{rad}=1/k_r$ between 7–297 K can be fitted to a three-states kinetic model (Figure 3B) according to Equation (1):

$$\tau_{rad}=\frac{3+\exp\left[-\frac{\Delta E(S_1-T_1)}{k_BT}\right]}{3k_{fl}+k_{ph}\cdot\exp\left[-\frac{\Delta E(S_1-T_1)}{k_BT}\right]} \quad (1)$$

providing an estimated $\Delta E(S_1\text{-}T_1)=79$ meV (637 cm^{-1}), which is in excellent agreement with the DFT/MRCI energy difference at the S_1 minimum in THF of 90 meV (726 cm^{-1}). The small energy gap and long lifetime of the T_1 state of ca. 6 ms (calc. 32 ms) are beneficial for efficient rISC, and in combination with the estimated short $\tau(S_1)=22$ ns, efficient TADF is enabled.

An anomalous hypsochromic shift of the emission in CH_2Cl_2 by ca. 100 nm upon cooling to 77 K is observed (Table 1), which appears to originate from a population of a different excited state. In addition to the ^{3}LLCT state, we find a higher-lying minimum on the T_1 potential energy surface that is of ^{3}LC(dbt) nature (Figure 3D and Figure S31). The involvement of the sulfur atoms in the excitation mediates SOC (64 cm^{-1}, Table S9), resulting in phosphorescence with $\tau_{rad}=22$ ms according to the calculations.

Transient absorption (TA) studies of **Zn1** in toluene (Figure 4) confirm that internal conversion and ISC leading to the formation of the final ^{3}LL/LMCT state, that is involved in the TADF process, occur on a timescale faster than our instrument response of 10 ns. The TA spectrum shows in general a positive absorbance change over the whole spectral range with a drop in optical density at $\lambda_{abs}=390$ and 320 nm, which coincides with overlapping ground state absorption. The decays of the excited state absorption (ESA) at $\lambda_{abs}=348$ and 440 nm were fitted monoexponentially and yielded lifetimes of 370 and 354 ns, respectively, which is in the range of the recorded luminescence lifetimes.

The population of triplet excited states, of which the broad emission covers an energy range from 2.48-1.60 eV, with associated long lifetimes of hundreds of nanoseconds in solution suggests that **Zn1** may be employed in photocatalytic transformations as triplet sensitizer, similar to two recently reported Zn(II) complexes with dark (non-emissive) triplet

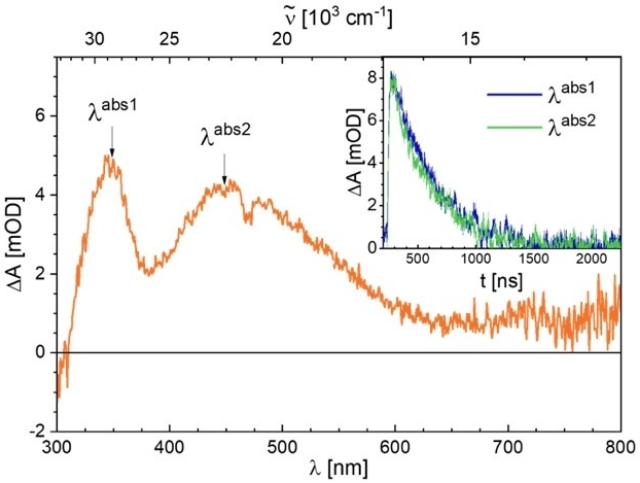

Figure 4. Transient absorption spectrum of **Zn1** in de-aerated toluene at 293 K, recorded at 10 ns time delay upon excitation at 420 nm with laser pulse energy of 15 mJ. The spectrum was recorded with an integration time of 100 ns after the indicated delay time. The inset shows the decays of the excited state absorption (ESA) signals at 348 nm (blue trace) and 440 nm (green trace).

excited states.[41] Fulfilling another important prerequisite for photocatalysis, the continuous irradiation of **Zn1** for one hour with high-power 450 nm LEDs revealed excellent photostability by maintaining 96% and 99% of the original absorbance in toluene and THF, respectively (Figure S24). The photo-isomerization (*E*)-stilbene→(*Z*)-stilbene requires the population of the organic T_1 state at 2.2 eV, of which sensitization with our zinc(II) complex appears feasible. Indeed, 2 mol-% of **Zn1** in degassed toluene give 93% conversion after four hours of irradiation, which is faster than found for the standard $[Ru(bpy)_3]^{3+}$ that requires 5 mol-% and 8 h.[42] Control experiments under identical conditions but without **Zn1** showed no formation of (*Z*)-stilbene (Figure S25), highlighting the suitability of our zinc(II) complex for photocatalytic transformations.

Conclusions

In conclusion, a new type of dimeric Zn^{II}-based emitter in the yellow to orange region of the electromagnetic spectrum, with a donor-M-acceptor motif by employing an electron-rich thiolate ligand in combination with an electrophilic carbene ligand, exhibits $^{1/3}$LLCT states suitable for efficient TADF with high k_r. The visible light absorption, for carbene complexes astonishing stability towards air and water, in combination with the observation of long-lived triplet states in solution renders the complex suitable for Dexter energy transfer photocatalysis. Overall, these promising first results clearly show that Zn^{II}-based photoactive complexes bear great potential as serious alternatives to traditional 4d and 5d transition metal compounds employed in devices and photochemistry.

Experimental Section

General considerations: All operations were performed under an argon atmosphere by using conventional Schlenk-line techniques or glovebox. The solvents were dried using Technology Inc. PureSolv system or standard methods, and were degassed and stored over activated 4 Å molecular sieves. Dimeric $[Zn_2(\mu\text{-}Cl)_2(Cl)_2(^{Me}cAAC)_2]$[37] and benzene-1,2-dithiol[43,44] (for details see below) were prepared according to established procedures. All other starting materials were available commercially and were used without further purification. ^1H, $^{13}C\{^1H\}$ APT, ^1H–^{13}C HSQC, ^1H–^{13}C HSMB, ^1H–^1H COSY and ^1H–^{15}N HMBC NMR spectra were measured at 300 K on Bruker 500 Avance or Bruker 600 Avance spectrometers. The chemical shifts are given in ppm relative to residual signals of the respective solvent [^1H, ^{13}C: CD_2Cl_2 (5.32, 53.84 ppm); C_6D_6 (7.16, 128.06)]. Cyclic voltammetry measurements were performed on a Gamry Instruments Reference [600] potentiostat with three electrodes cell configuration (working electrode: Pt-disk, counter electrode: Pt-wire, reference electrode: silver wire separated by Vycor tip). Redox potentials are referenced to the ferrocene/ferrocenium couple and $^nBu_4NBF_4$ was used (100 mM solution) as supporting electrolyte. TGA/DSC data were recorded using a STA650 instrument (TA instruments, USA) with a heat rate of 10 °C/min and under constant flow of nitrogen gas.

All photophysical measurements were performed in dry and deaerated solutions. In the case of polymeric matrices, the respective polymer (PMMA or PS) was weighted into a vial together with 10 wt% of **Zn1**. Subsequently, the mixture was dissolved in DCM, the solution was added to a spectroscopic cuvette, and the solvent was slowly evaporated to form a thin layer (film) of **Zn1** in the matrix. The remaining solvent molecules were evaporated by keeping the film under a low vacuum for 12 h. The solid-state measurements were performed either in single-crystalline form (sample denoted as 'crystals') or, to remove co-crystallized molecules of solvent, single-crystals were ground and dried under vacuum for 24 h (sample denoted as 'solid'). Optical absorption spectroscopy was performed using an Agilent Cary 5000 spectrophotometer using standard 1 cm path length quartz cells. Excitation and emission spectra were recorded on an Edinburgh Instrument FLS1000 spectrometer, equipped with a 450 W Xenon arc lamp, double monochromators for the excitation and emission pathways, and a red-sensitive photomultiplier (PMT-980) as a detector. The excitation and emission spectra were corrected using the standard corrections supplied by the manufacturer for the excitation source's spectral power and the detector's sensitivity. Quantum yields in solution were measured using an FLS1000 spectrometer equipped with an integrating sphere (N-M01), and the quantum yield of solid samples and polymeric matrices were measured using an integrating cryosphere (Microstat N2) from Oxford Instruments. The luminescence lifetimes were measured using a μF2 pulsed 60 W Xenon microsecond flashlamp, with a repetition rate of 100 Hz and a multichannel scaling (MCS) module or with VPLEDs (383.8 nm with 1.1 mW or 449.6 nm with 37 mW), with 100 ns pulse width and an MCS module, depending on the time range. The emission was collected at a right angle to the excitation source. The low-temperature experiments were performed using liquid nitrogen-cooled OptistatDN-V cryostat from Oxford Instruments or 4 K cryostat (CS204SI-FMX-1SS) from Advanced Research System equipped with a closed cycle water-cooled helium compressor.

An LP920-KS apparatus from Edinburgh Instruments was employed for nanosecond transient absorption spectroscopy. Excitation was performed by a frequency-tripled Nd:YAG laser (Quantel Brilliant b, ca. 10 ns pulse width and ca. 10 mJ output) equipped with an OPO from Opotek (excitation wavelength set to 420 nm with ca. 15 mJ output). A beam expander (GBE02-A from Thorlabs) was used to ensure homogeneous excitation. Detection of transient absorption spectra occurred on an iCCD camera (Andor), whereas kinetics at a single wavelength were recorded using a photomultiplier tube. Samples were prepared in toluene (50 μM), degassed by rigorous bubbling with dry Ar, and checked for photodegradation via UV/VIS in regular intervals over the course of the measurements.

Preliminary picosecond transient absorption studies with sub-nanosecond time resolution were performed using a TRASS instrument from Hamamatsu and a mode-locked picosecond Nd:YAG laser (model PL2251B-10-SH-TH with PRETRIG option) as an excitation source. The laser pulse duration was ~30 ps and the pulse frequency was 10 Hz. The third harmonic (355 nm) was used for excitation of the sample, however, significant decomposition was observed over the course of the measurement, presumably due to the high energy (both pulse energy and wavelength) of the excitation source.

Computational Methods: For all geometry optimizations the Gaussian 16 program was used.[45] The ground state geometries were optimized with Kohn–Sham density functional theory (DFT).[46] For the optimization of the singlet excited state geometries the time dependent DFT (TDDFT)[47] was used and for the excited triplet state geometries the Tamm-Dancoff approximation (TDA)[48] to TDDFT was chosen. The 10-mdf 6 s5p3d basis set with defpp-ecp was used for the zinc atoms[49] and for sulfur the def2-SVPD basis was chosen.[50] For all other atoms the def-SV(P) basis set was used.[50] As functional BH-LYP functional was chosen for all calculations.[51,52] A THF environment was mimicked via the polarizable continuum model (PCM).[53,54] To examine the excitation energies and oscillator strengths of the spin allowed transitions, DFT/MRCI calculations were carried out.[55,56] As Hamiltonian, the redesigned R2018 was selected and 30 singlet and 30 triplet roots were calculated. For the DFT/MRCI calculations, the point charges of the Gaussian 16 calculations were extracted. With the SPOCK program, the spin-orbit coupling matrix elements (SOCMEs) were obtained.[57,58]

Synthetic Procedures

$C_6H_4S_2H_2$ (H_2bdt): 5 mL of benzenethiol (49 mmol) were added dropwise to a mixture of *n*-BuLi (103 mmol, 2.5 M, 41 mL) and TMEDA (54 mmol, 8.1 mL) in 40 mL of *n*-pentane at −78 °C. The mixture was allowed to slowly warm to room temperature and stirred overnight. Then the solution was again cooled to −78 °C and octasulfur (49 mmol) was added dropwise. The mixture was stirred at −78 °C for two hours and overnight at room temperature, followed by slow addition of 10 mL of water. The quenched mixture was poured into diluted hydrochloric acid and extracted with Et_2O (3×50 mL). Organic layers were combined, dried over anhydrous $MgSO_4$ and evaporated to dryness using rotavapor. The crude product was vacuum distilled (55 °C, 0.2 mbar) to give 1.4 mL (24%) of colorless liquid. ^1H NMR (500 MHz, C_6D_6): 7.96 (m, 2H), 6.65 (m, 2H), 3.35 (s, 2H). ^{13}C NMR (125 MHz, C_6D_6): 131.4 (s, 2 C), 130.9 (s, 2 C), 126.4 (s, 2 C).

$C_6H_4S_2Na_2$ (bdt): 337 mg (14 mmol) of NaH was dispersed in 20 mL of THF and 1.1 g (7.7 mmol) of benzene-1,2-dithiol in 10 mL of THF was added dropwise. After complete addition, the mixture was stirred for one hour at 60 °C and then overnight at room temperature. After filtration, the remaining white solid was washed with additional portion of THF (2×15 mL) and the

product was vacuum-dried for 4 h at 60 °C. Yield: 942 mg (5.0 mmol, 72 %) of white powder.

[(^{Me}cAAC)Zn(k*S*:μ^2*S*-PhS$_2$)$_2$Zn(^{Me}cAAC)] (Zn1): 47 mg of (250 mmol) disodium benzene-1,2-dithiolate (**bdt**) was mixed with 100 mg (119 mmol) of [(^{Me}cAAC)(Cl)Zn(μ-Cl)$_2$Zn(Cl)(^{Me}cAAC)] in 7 mL of THF and the resulting mixture was stirred overnight at room temperature. After that, the solvents were vacuum-evaporated, and the solid residue was extracted with DCM (3x5 mL). The combined organic fractions were concentrated by vacuum evaporation to a final volume of 3 mL and crystallization was induced by gas phase diffusion of n-pentane. The obtained single-crystals were collected, washed with cold THF (2 mL), *n*-pentane (2×5 mL) and vacuum dried. Yield: 86 mg (73.5 %, 86 mmol) of yellow crystalline material. CHNS analysis calcd for $C_{53}H_{72}N_2S_4ZnCl_2$: C, 59.7; H, 6.8; N, 2.6. Found: C, 59.8; H, 7.1; N, 2.62. ^{1}H NMR (600 MHz, CD_2Cl_2): δ [ppm] = 7.53 (t, $^3J(^1H,^1H)$ = 7.8 Hz, 2H, H^4, $C_6H_3^iPr_2$), 7.39 (m, 4H, $C_6H_4S_2$), 7.35 (d, $^3J(^1H,^1H)$ = 7.8 Hz, 4H, H^{3,5}, $C_6H_3^iPr_2$), 6.69 (m, 4H, $C_6H_4S_2$), 2.77 (sept, $^3J(^1H,1H)$ = 6.7 Hz, 4H, C*H*^{iPr}), 2.17 (s, 4H, −CH_2−), 1.57 (s, 12H, (CH_3)$_2$), 1.48 (s, 12H, (CH_3)$_2$), 1.32 (d, $^3J(^1H,1H)$ = 6.7 Hz, 12H, CH_3^{iPr}), 1.23 d, $^3J(^1H,^1H)$ = 6.7 Hz, 12H, CH_3^{iPr}). ^{13}C NMR (125 MHz, CD_2Cl_2): δ [ppm] = 243.8 (s, 2 C, *C*^{carbene}), 145.2 (s, 4 C, C^{2,6}, *Dipp*), 144.4 (s, 4 C, C^{1,2}, *Ph*S$_2$), 133.9 (s, 2 C, C^1, *Dipp*), 130.9 (s, 2 C, C^4, *Dipp*), 130.6 (s, 4 C, *Ph*S$_2$), 126.1 (s, 4 C, C^{3,5}, *Dipp*), 122.3 (s, 4 C, *Ph*S$_2$), 84.5 (s, 2 C, NC*C*^{carbene}), 55.2 (s, 2 C, N*C*(CH$_3$)$_2$), 49.9 (s, 2 C, -CH_2−), 29.5 (s, 4 C, C(*C*H$_3$)$_2$), 29.4 (s, 4 C, *C*H(CH$_3$)$_2$, Dipp), 28.1 (s, 4 C, C(*C*H$_3$)$_2$), 27.3 (s, 4 C, CH(*C*H$_3$)$_2$, Dipp), 23.9 (s, 4 C, CH(*C*H$_3$)$_2$, Dipp). ^{15}N (60 MHz, CD_2Cl_2): δ [ppm] = -141.86 ppm.

Deposition Number 2189606 (for **Zn1**) contains the supplementary crystallographic data for this paper. These data are provided free of charge by the joint Cambridge Crystallographic Data Centre and Fachinformationszentrum Karlsruhe Access Structures service.

Acknowledgements

This work was supported by Deutsche Forschungsgemeinschaft [DFG, Priority Program SPP 2102 "Light-controlled reactivity of metal complexes" (MA 1051/18-1 and STE 1834/7-1)]. We are also grateful to the DFG for funding of major research equipment (INST 212/430-1 FUGG and INST 212/455-1 FUGG). A.B. is grateful to Alexander von Humboldt Foundation for a Research Fellowship grant for Postdoctoral Research. C.W. acknowledges the Deutsche Forschungsgemeinschaft (DFG, German Research Foundation) for the funding (WA 5012/1-1). Open Access funding enabled and organized by Projekt DEAL.

Conflict of Interest

The authors declare no conflict of interest.

Data Availability Statement

The data that support the findings of this study are available in the supplementary material of this article.

Keywords: carbenes · luminescence · photocatalysis · TADF · zinc

[1] C. Förster, K. Heinze, *Chem. Soc. Rev.* **2020**, *49*, 1057–1070.
[2] O. S. Wenger, *J. Am. Chem. Soc.* **2018**, *140*, 13522–13533.
[3] C. B. Larsen, O. S. Wenger, *Chem. Eur. J.* **2018**, *24*, 2039–2058.
[4] C. Wegeberg, O. S. Wenger, *JACS Au* **2021**, *1*, 1860–1876.
[5] B. M. Hockin, C. Li, N. Robertson, E. Zysman-Colman, *Catal. Sci. Technol.* **2019**, *9*, 889–915.
[6] A. Steffen, B. Hupp, in Comprehensive Coordination Chemistry III (Eds.: E. C. Constable, G. Parkin, L. Que Jr), Elsevier, Oxford, **2021**, pp. 466–502.
[7] O. S. Wenger, *Chem. Rev.* **2013**, *113*, 3686–3733.
[8] Q. Zhao, C. Huang, F. Li, *Chem. Soc. Rev.* **2011**, *40*, 2508–2524.
[9] C. Bizzarri, E. Spuling, D. M. Knoll, D. Volz, S. Bräse, *Coord. Chem. Rev.* **2018**, *373*, 49–82.
[10] R. Hamze, J. L. Peltier, D. Sylvinson, M. Jung, J. Cardenas, R. Haiges, M. Soleilhavoup, R. Jazzar, P. I. Djurovich, G. Bertrand, M. E. Thompson, *Science* **2019**, *363*, 601–606.
[11] J. X. Wang, C. Li, H. Tian, *Coord. Chem. Rev.* **2021**, *427*, 213579.
[12] J.-H. Shon, D. Kim, M. D. Rathnayake, S. Sittel, J. Weaver, T. S. Teets, *Chem. Sci.* **2021**, *12*, 4069–4078.
[13] C. K. Prier, D. A. Rankic, D. W. C. MacMillan, *Chem. Rev.* **2013**, *113*, 5322–5363.
[14] D. M. Arias-Rotondo, J. K. McCusker, *Chem. Soc. Rev.* **2016**, *45*, 5803–5820.
[15] J. K. McCusker, *Science* **2019**, *363*, 484–488.
[16] P. Chábera, Y. Liu, O. Prakash, E. Thyrhaug, A. El Nahhas, A. Honarfar, S. Essén, L. A. Fredin, T. C. B. Harlang, K. S. Kjær, K. Handrup, F. Ericson, H. Tatsuno, K. Morgan, J. Schnadt, L. Häggström, T. Ericsson, A. Sobkowiak, S. Lidin, P. Huang, S. Styring, J. Uhlig, J. Bendix, R. Lomoth, V. Sundström, P. Persson, K. Wärnmark, *Nature* **2017**, *543*, 695–699.
[17] S. Otto, M. Grabolle, C. Förster, C. Kreitner, U. Resch-Genger, K. Heinze, *Angew. Chem. Int. Ed.* **2015**, *54*, 11572–11576; *Angew. Chem.* **2015**, *127*, 11735–11739.
[18] S. B. Vittardi, R. T. Magar, B. R. Schrage, C. J. Ziegler, E. Jakubikova, J. J. Rack, *Chem. Commun.* **2021**, *57*, 4658–4661.
[19] Y. Zhang, T. S. Lee, J. M. Favale, D. C. Leary, J. L. Petersen, G. D. Scholes, F. N. Castellano, C. Milsmann, *Nat. Chem.* **2020**, *12*, 345–352.
[20] M. Gernert, U. Müller, M. Haehnel, J. Pflaum, A. Steffen, *Chem. Eur. J.* **2017**, *23*, 2206–2216.
[21] M. Gernert, L. Balles-Wolf, F. Kerner, U. Müller, A. Schmiedel, M. Holzapfel, C. M. Marian, J. Pflaum, C. Lambert, A. Steffen, *J. Am. Chem. Soc.* **2020**, *142*, 8897–8909.
[22] R. Hamze, S. Shi, S. C. Kapper, D. S. Muthiah Ravinson, L. Estergreen, M.-C. Jung, A. C. Tadle, R. Haiges, P. I. Djurovich, J. L. Peltier, R. Jazzar, G. Bertrand, S. E. Bradforth, M. E. Thompson, *J. Am. Chem. Soc.* **2019**, *141*, 8616–8626.
[23] A. M. T. Muthig, M. Krumrein, J. Wieland, M. Gernert, F. Kerner, J. Pflaum, A. Steffen, *Inorg. Chem.* **2022**, *61*, 14833–14844.
[24] V. A. Krylova, P. I. Djurovich, B. L. Conley, R. Haiges, M. T. Whited, T. J. Williams, M. E. Thompson, *Chem. Commun.* **2014**, *50*, 7176–7179.
[25] B. Hupp, C. Schiller, C. Lenczyk, M. Stanoppi, K. Edkins, A. Lorbach, A. Steffen, *Inorg. Chem.* **2017**, *56*, 8996–9008.
[26] B. Hupp, J. Nitsch, T. Schmitt, R. Bertermann, K. Edkins, F. Hirsch, I. Fischer, M. Auth, A. Sperlich, A. Steffen, *Angew. Chem. Int. Ed.* **2018**, *57*, 13671–13675; *Angew. Chem.* **2018**, *130*, 13860–13864.
[27] J. Nitsch, F. Lacemon, A. Lorbach, A. Eichhorn, F. Cisnetti, A. Steffen, *Chem. Commun.* **2016**, *52*, 2932–2935.
[28] A. Ruduss, B. Turovska, S. Belyakov, K. A. Stucere, A. Vembris, K. Traskovskis, *Inorg. Chem.* **2022**, *61*, 2174–2185.
[29] R. Tang, S. Xu, T.-L. Lam, G. Cheng, L. Du, Q. Wan, J. Yang, F.-F. Hung, K.-H. Low, D. L. Phillips, C.-M. Che, *Angew. Chem. Int. Ed.* **2022**, *61*, e202203982.
[30] S. Bestgen, C. Schoo, B. L. Neumeier, T. J. Feuerstein, C. Zovko, R. Köppe, C. Feldmann, P. W. Roesky, *Angew. Chem. Int. Ed.* **2018**, *57*, 14265–14269; *Angew. Chem.* **2018**, *130*, 14461–14465.

[31] R. Sakamoto, T. Iwashima, J. F. Kögel, S. Kusaka, M. Tsuchiya, Y. Kitagawa, H. Nishihara, *J. Am. Chem. Soc.* **2016**, *138*, 5666–5677.
[32] J. F. Kögel, S. Kusaka, R. Sakamoto, T. Iwashima, M. Tsuchiya, R. Toyoda, R. Matsuoka, T. Tsukamoto, J. Yuasa, Y. Kitagawa, T. Kawai, H. Nishihara, *Angew. Chem. Int. Ed.* **2016**, *55*, 1377–1381; *Angew. Chem.* **2016**, *128*, 1399–1403.
[33] K. A. Truesdell, G. A. Crosby, *J. Am. Chem. Soc.* **1985**, *107*, 1787–1788.
[34] N. Lüdtke, J. Kuhnt, T. Heil, A. Steffen, C. M. Marian, *ChemPhotoChem* **2022**, *7*, e202200142.
[35] B. Goswami, T. J. Feuerstein, R. Yadav, S. Lebedkin, P. J. Boden, S. T. Steiger, G. Niedner-Schatteburg, M. Gerhards, M. M. Kappes, P. W. Roesky, *Chem. Eur. J.* **2021**, *27*, 15110–15119.
[36] Y. Sakai, Y. Sagara, H. Nomura, N. Nakamura, Y. Suzuki, H. Miyazaki, C. Adachi, *Chem. Commun.* **2015**, *51*, 3181–3184.
[37] O. Mrózek, M. Gernert, A. Belyaev, M. Mitra, L. Janiak, C. M. Marian, A. Steffen, *Chem. Eur. J.* **2022**, *28*, e202201114.
[38] K. Halvorsen, G. A. Crosby, W. F. Wacholtz, *Inorg. Chim. Acta* **1995**, *228*, 81–88.
[39] D. M. Hatch, W. F. Wacholtz, J. T. Mague, *Acta Crystallogr. Sect. C* **2003**, *59*, m452-m453.
[40] M. Borsari, M. Cannio, G. Gavioli, *Electroanalysis* **2003**, *15*, 1192–1197.
[41] J. A. Kübler, B. Pfund, O. S. Wenger, *JACS Au* **2022**, *2*, 2367–2380.
[42] M. M. Floes-Leonar, C. R. Azpilcueta, C. Amador-Bedolla, S. S. Rozenel, *J. Photochem. Photobiol. A* **2021**, *414*, 113224.
[43] P. S. Nejman, B. Morton-Fernandez, N. Black, D. B. Cordes, A. M. Slawin, P. Kilian, J. D. Woollins, *J. Organomet. Chem.* **2015**, *776*, 7–16.
[44] D. M. Giolando, K. Kirschbaum, *Synthesis* **1992**, 451–452.
[45] Gaussian 16, Revision A.03, M. J. Frisch, G. W. Trucks, H. B. Schlegel, G. E. Scuseria, M. A. Robb, J. R. Cheeseman, G. Scalmani, V. Barone, G. A. Petersson, H. Nakatsuji et al., 2016; Gaussian Inc. Wallingford CT.
[46] M. Von Arnim, R. Ahlrichs, *J. Comput. Chem.* **1998**, *19*, 1746–1757.
[47] F. Furche, R. Ahlrichs, *J. Chem. Phys.* **2002**, *117*, 7433–7447.
[48] S. Hirata, M. Head-Gordon, *Chem. Phys. Lett.* **1999**, *314*, 291–299.
[49] D. Figgen, G. Rauhut, M. Dolg, H. Stoll, *Chem. Phys.* **2005**, *311*, 227–244.
[50] A. Schäfer, H. Horn, R. Ahlrichs, *J. Chem. Phys.* **1992**, *97*, 2571–2577.
[51] C. Lee, W. Yang, R. G. Parr, *Phys. Rev. B* **1988**, *37*, 785–789.
[52] A. D. Becke, *J. Chem. Phys.* **1993**, *98*, 1372–1377.
[53] E. Cancès, B. Mennucci, J. Tomasi, *J. Chem. Phys.* **1997**, *107*, 3032.
[54] B. Mennucci, E. Cancès, J. Tomasi, *J. Phys. Chem. B* **1997**, *101*, 10506.
[55] S. Grimme, M. Waletzke, *J. Chem. Phys.* **1999**, *111*, 5645–5655.
[56] C. M. Marian, A. Heil, M. Kleinschmidt, *WIREs Comput. Mol. Sci.* **2019**, *9*, e1394.
[57] M. Kleinschmidt, J. Tatchen, C. M. Marian, *J. Comput. Chem.* **2002**, **23**, 824–833.
[58] M. Kleinschmidt, C. M. Marian, *Chem. Phys.* **2005**, *311*, 71–79.

Manuscript received: December 20, 2022
Accepted manuscript online: January 13, 2023
Version of record online: March 15, 2023